Solar Energy xxx (xxxx) xxx–xxx

Contents lists available at ScienceDirect

Solar Energy

journal homepage: www.elsevier.com/locate/solener

Interdigitated back contact silicon heterojunction solar cells featuring an interband tunnel junction enabling simplified processing

B. Paviet-Salomon[a,*], A. Tomasi[b], D. Lachenal[c], N. Badel[a], G. Christmann[a], L. Barraud[a], A. Descœudres[a], J. Geissbühler[a], A. Faes[a], Q. Jeangros[b], J.P. Seif[b], S. Nicolay[a], B. Strahm[c], S. De Wolf[b,1], C. Ballif[a,b], M. Despeisse[a]

[a] CSEM, PV-Center, Rue Jaquet-Droz 1, CH-2002 Neuchâtel, Switzerland
[b] Photovoltaics and Thin-Film Electronics Laboratory, IMT, EPFL, Maladière 71B, CH-2000 Neuchâtel, Switzerland
[c] Meyer Burger Research SA, Rouges-Terres 61, CH-2022 Hauterive, Switzerland

ARTICLE INFO

Keywords:
Passivating contacts
Interdigitated back contact
Tunnel junction
Silicon solar cells

ABSTRACT

This paper reports on the development of an innovative back-contacted crystalline silicon solar cell with passivating contacts featuring an interband tunnel junction at its electron-collecting contacts. In this novel architecture, named "tunnel-IBC", both the hole collector patterning and its alignment to the electron collector are eliminated, thus drastically simplifying the process flow. However, two prerequisites have to be fulfilled for such devices to work efficiently, namely (i) lossless carrier transport through the tunnel junction and (ii) low lateral conductance within the hole collector in order to avoid shunts with the neighboring electron-collecting regions. We meet these two contrasting requirements by exploiting the anisotropic and substrate-dependent growth mechanism of n- and p-type hydrogenated nano-crystalline silicon layers. We investigate the influence of the deposition temperature and the doping gas concentration on the structural and the selectivity properties of these layers. Eventually, tunnel-IBC devices integrating hydrogenated nano-crystalline silicon layers demonstrate a conversion efficiency up to 23.9%.

1. Introduction

As the efficiency of single junction crystalline silicon-based solar cells steadily approaches their theoretical limit (Richter et al., 2013), establishing new records increasingly requires to diligently identify and mitigate the remaining optical and electrical loss mechanisms. Along these lines, the combination of a back-contacted design with passivating contacts has been anticipated in the last couple of years to be the ideal solar cell structure, as it combines a shadow loss-free front side – enabling a high short-circuit current density – together with a high open-circuit voltage enabled by well-passivated contacts. In this context, Panasonic, Japan, reported in 2014 on a 25.6%-efficient back-contacted crystalline silicon solar cell using an amorphous/crystalline silicon heterojunction (SHJ) as passivating contact material (Masuko et al., 2014), breaking the long lasting record of the UNSW PERC solar cell (Zhao et al., 1998) and convincingly demonstrating the potential of back-contacted devices with passivating contacts. Soon afterwards, still using hydrogenated amorphous silicon (*a*-Si:H) as passivating materials, Kaneka, Japan, successively released in 2016 and 2017 three back-contacted devices, all with efficiencies beyond 26.0% (Yoshikawa et al., 2016, 2017a, 2017b). This race to record efficiency culminated with the demonstration by Kaneka, Japan, of an impressive 26.7%-efficient back-contacted solar cell (Green et al., 2017). Equally interesting, ISFH, Germany (Krügener et al., 2017), and SunPower, USA (Green et al., 2016), recently broke the 25.0% efficiency barrier with back-contacted devices, but using a silicon oxide and polysilicon stack as passivating contact materials.

In spite of these outstanding results, it is commonly accepted that back-contacted devices suffer from complex processing, which is unfavorable for mass production. This increased process complexity stems from the need to individually pattern and accurately align the electron- and the hole-collecting regions (usually in the form of two interdigitated combs), their respective electrode, as well as opened regions ("gaps") to prevent shunts between the two polarities. Important efforts have thus been devoted to develop industry-compatible patterning techniques, such as direct laser ablation (Harrison et al., 2016), dry etching (Kim et al., 2017; Tucci et al., 2008), and their combination (Xu et al., 2017), as well as shadow masking (Tomasi et al., 2014a, 2014b).

* Corresponding author.
E-mail address: bertrand.paviet-salomon@csem.ch (B. Paviet-Salomon).
[1] Now with King Abdullah University of Science and Technology (KAUST), KAUST Solar Center (KSC), Thuwal 23955-6900, Saudi Arabia.

https://doi.org/10.1016/j.solener.2018.01.066
Received 30 October 2017; Received in revised form 17 January 2018; Accepted 19 January 2018
0038-092X/

These methods aim at replacing the photolithography still used (sometimes allegedly) for best-in-class back-contacted devices (Krügener et al., 2017; Masuko et al., 2014; Yoshikawa et al., 2017a,b).

Regardless of the chosen patterning technique, an important part of the process complexity is a consequence of the accurate alignments required at several stages of a back-contacted device fabrication, namely the alignment of the electron- *vs* the hole-collecting fingers and of their respective electrode. Consequently, a dramatic alleviation of the process complexity can be expected from simplifying the device architecture itself. Several papers already pointed out that a gap between the electron- and the hole-collecting regions is not needed, already relaxing the alignment constraints (Noge et al., 2015; Stang et al., 2017; Tomasi et al., 2014b). Going even further, we proposed recently (Tomasi et al., 2017) a disruptive back-contacted device architecture featuring an interband silicon tunnel junction at the electron-collecting regions. This innovative approach, named "tunnel-IBC", dramatically simplifies the process flow of back-contacted devices as it eliminates the patterning of the hole collector as well as its alignment to the electron collector, and might thus be a major leap towards their cost-effective production.

In this contribution, we provide further insights into the tunnel-IBC architecture, and especially focus on the development of efficient tunnel junctions and hole collectors using hydrogenated nano-crystalline silicon (*nc*-Si:H) layers.

2. The tunnel-IBC device: Architecture and challenges

Fig. 1 compares the architecture of a conventional interdigitated back contact silicon heterojunction (IBC-SHJ) device and the tunnel-IBC concept. In a conventional IBC-SHJ device, both the electron and the hole collectors are patterned and must be aligned one with respect to the other. In contrast, in the tunnel-IBC device, only the electron collector is patterned, whereas the hole collector covers the entire rear surface, including the electron-collecting fingers, hence forming a tunnel junction (TJ) at these locations.

Compared to conventional IBC-SHJ devices, the tunnel-IBC relies on a drastically simplified process flow. Indeed, it simultaneously eliminates the requirement of any patterning step for the hole-collecting regions, as well as any alignment between the hole- and the electron-collecting regions. Consequently, only two patterning steps and one alignment step are required, namely (i) the patterning of the electron-collecting fingers, (ii) the patterning of the TCO/metal electrode, and (iii) the alignment of the patterned TCO/metal electrode on the electron- and the hole-collecting regions. This very lean process flow is thus an important progress towards the successful implementation of the IBC-SHJ technology at industrial level.

However, in order to work efficiently, the tunnel-IBC device must overcome some challenges. First, the TJ located at the electron-collecting regions must offer a good electron selectivity and not impede the carrier transport to the back electrode. A well-known possibility to do so is to use highly-doped materials in order to narrow the TJ depletion width, and hence facilitate the tunneling of the carriers (Esaki, 1958). Second, as the hole collector covers the entire rear surface, the hole- and the electron-collecting regions are electrically connected. To prevent lateral carrier transport – and hence short-circuits – the hole collector materials must feature a low lateral conductance. Importantly, this second requirement is in apparent contrast with the first one, where a high doping – and hence a high conductivity – is required. As already developed in (Tomasi et al., 2017), we exploited the anisotropic growth mechanism of *nc*-Si:H layers to fulfil these two competing requirements. In Section 4 below, additional insights into the required properties of the *nc*-Si:H layers will be provided and discussed.

3. Experimental

3.1. *a-Si:H and nc-Si:H layers characterization*

The thickness of the *a*-Si:H and the *nc*-Si:H layers was measured on glass samples by spectroscopic ellipsometry using a J.A. Woolam α-SE™ tool. The crystallinity of the *nc*-Si:H layers was determined by Raman spectroscopy using a Renishaw inVia tool operated with a 515 nm laser. Again, glass samples, coated either with a single 10-nm-thick intrinsic *a*-Si:H substrate layer or with a stack comprising the former 10-nm-thick *a*-Si:H(i) layer capped with an additional 50-nm-thick n-type *nc*-Si:H layer, were used. The Raman spectra were fitted using three Gaussian peaks centered at 480 cm^{-1}, 510 cm^{-1} and 520 cm^{-1}. The Raman crystallinity (χ_c) was then calculated as $\chi_c = (A_{510} + A_{520})/(A_{480} + A_{510} + A_{520})$ where A_{480} (resp. A_{510} and A_{520}) represents the area below the Gaussian peak at a wavenumber of 480 nm^{-1} (resp. 510 nm^{-1} and 520 nm^{-1}), as proposed by (Vallat-Sauvain et al., 2006). Note that the penetration depth of the 515 nm laser used here in *nc*-Si:H is of about 50 nm (Carpenter et al., 2017), which is comparable to the typical thickness of the *nc*-Si:H layers under investigation. Consequently, the Raman crystallinity calculated in this contribution is an average value over the whole layer thickness. The microstructure of the *a*-Si:H/*nc*-Si:H hole and electron contacts was assessed by transmission electron microscopy (TEM) using a probe and image Cs-corrected FEI Titan microscope operated at 200 kV. For that purpose, cross-sections of the two contacts were prepared using the conventional focused ion beam lift-out method in a Zeiss NVision 40 workstation.

3.2. *Device processing*

Three kinds of devices were considered in this paper. First, to conduct the preliminary developments of the *nc*-Si:H layers, 4-cm^2 two side-contacted silicon heterojunction solar cells with front hole collector (FHC, sometimes still referred to as "front emitter") were processed. Two arrangements of these FHC devices were investigated. In a first arrangement ("FHC type I" devices, see Fig. 2), the devices featured an intrinsic/p-type *a*-Si:H stack at the front, whereas different full area TJ materials were investigated at the back, namely *a*-Si:H(n)/*a*-Si:H(p), *nc*-Si:H(n)/*a*-Si:H(p) and *nc*-Si:H(n)/*nc*-Si:H(p) stacks. These devices aimed at investigating the electron selectivity and transport properties

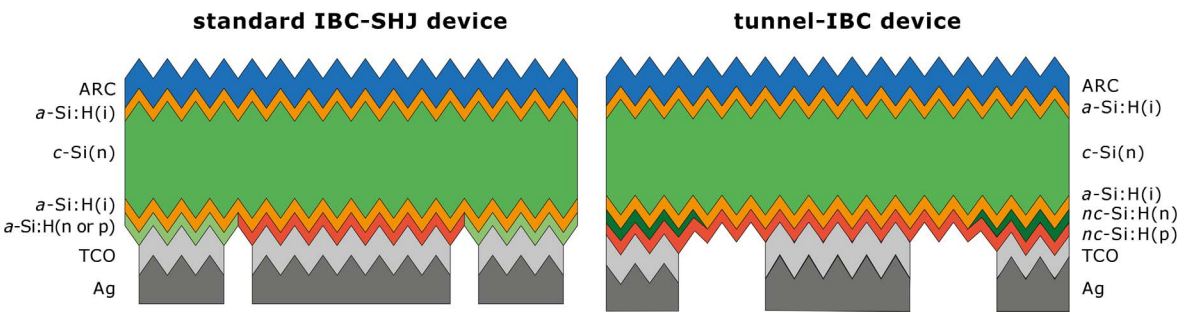

Fig. 1. Cross-section view of a conventional IBC-SHJ device (left) and the tunnel-IBC concept (right). Pictures adapted from (Tomasi et al., 2017).